A Density Functional Study of the Optical Spectra and Nonlinear Optical Properties of Heteroleptic Tetrapyrrole Sandwich Complexes: The Porphyrinato−Porphyrazinato−Zirconium(IV) Complex as a Case Study

G. Ricciardi and A. Rosa*

Dipartimento di Chimica, Università della Basilicata, Via N. Sauro 85, 85100 Potenza, Italy

S. J. A. van Gisbergen and E. J. Baerends*

Afdeling Theoretische Chemie, Vrije Universiteit, De Boelelaan 1083, 1081 HV Amsterdam, The Netherlands

Received: August 19, 1999; In Final Form: November 8, 1999

Time-dependent density functional theory calculations are presented for the excitation energies and oscillator strengths of the title mixed sandwich. They prove to agree very well with the experimental data, providing that an accurate description of the salient features of the UV−vis spectrum is given. The nature of the excitations, intraligand (excitonic) or interligand (charge-resonance), is discussed and compared to previous theoretical deductions for bisporphyrins. An experimental measurement of the first hyperpolarizability $\beta(-2\omega; \omega, \omega)$, related to a second harmonic generation, yielded a large, negative β at $\omega = 0.65$ eV and, by extrapolation, also a large, negative static value. This suggests that this complex has very interesting nonlinear optical properties. Our calculations, however, show β to have a pole very close to the laser frequency used in the experiment, with large, negative β values only in its vicinity. Off-resonance values of β at $\omega < 0.6$ eV are small and positive.

1. Introduction

Tetrapyrrole sandwich complexes have attracted considerable interest because they are good structural and spectroscopic models of the bacteriochlorophyll "special pair" in the reaction center of photosynthesis.[1] The metal ion in a sandwich complex holds the macrocycles closer together than their van der Waals distance, resulting in strong $\pi-\pi$ interactions that mimic the electronic interactions that occur within the special pair. These interactions are thought to be responsible for some of the peculiar properties of sandwich complexes, such as the ease of porphyrin π-system oxidation and the low energy of the first singlet (π, π^*) excited state, as compared to corresponding monomeric chromophores. This latter property produces a bathochromic shift in the long-wavelength absorption band and makes the dimer an effective trap for the harvested photon energy.

As a matter of fact, to date, a number of synthetic sandwich complexes, both homoleptic (in which the two tetrapyrroles are identical)[2−17] and heteroleptic (in which the two tetrapyrroles are different),[18−26] exist whose optical characteristics resemble those of the lowest excited states of the "special pair".

The homoleptic sandwiches have characteristic optical properties that include (i) momomer-like ground state absorption features, the Q and B bands, the latter being slightly blue-shifted compared to the monomer, (ii) a new Q″ absorption band at higher energy and a Q′ absorption band at lower energy than the monomer Q-bands, (iii) a broad, weak Q′ fluorescence band substantially red shifted from the Q′ absorption maximum, and (iv) a phosphorescence band significantly red-shifted from those of typical monoporphyrin complexes.[2]

The optical spectra of heteroleptic tetrapyrrole sandwiches show, besides the Q, Q′, and Q″ features typical of the homoleptic complexes, two main features in the UV region that have been assigned to the Soret bands of the subunits, on the basis of their correspondence to the Soret bands in homo sandwiches.[20,22] The essential features of the electronic spectra of homoleptic sandwiches have been interpreted by semiempirical configuration interaction (CI) approaches using both the localized molecular orbital (LO) basis[27−29] and the canonical molecular orbital (MO) basis.[2,29−34] Using the LO basis, the excited states of the dimer are described as linear combinations of intra- and interligand transitions, that is, exciton coupling (EX) and charge resonance (CR) configurations. The use of a canonical molecular orbital basis involves the construction of supermolecule (sandwich) MOs from linear combinations of the subunit MOs. The excited states are then described as linear combinations (CI) of the excited configurations obtained by considering the electron transitions from occupied to unoccupied supermolecule MOs. The supermolecule MO approach has also been used to describe the optical properties of strongly coupled π systems such as aromatic hydrocarbon excimers,[35] paracyclophanes,[36] and the reaction center special pair.[37,38] Because the localized molecular orbital and canonical molecular orbital bases are related by a unitary transformation, the two approaches are mathematically equivalent.

For homoleptic complexes, a simple supermolecule MO/CI model that readily explains the steady and the time-resolved electronic spectra of neutral bisporphyrin complexes has been proposed by Holten et al.[2,30]

According to this model, the supermolecule MOs are formed by taking bonding and antibonding linear combinations of the monomer a_{1u} (π) and a_{2u} (π) HOMOs and e_g (π^*) LUMOs of Gouterman's four-orbital model[39,40] that have been so successful in describing the electronic states of monoporphyrins. However, more accurate methods are required to achieve a detailed, quantitative understanding. [41−43] One electron promotion among

10.1021/jp9929216 CCC: $19.00
Published on Web 12/29/1999

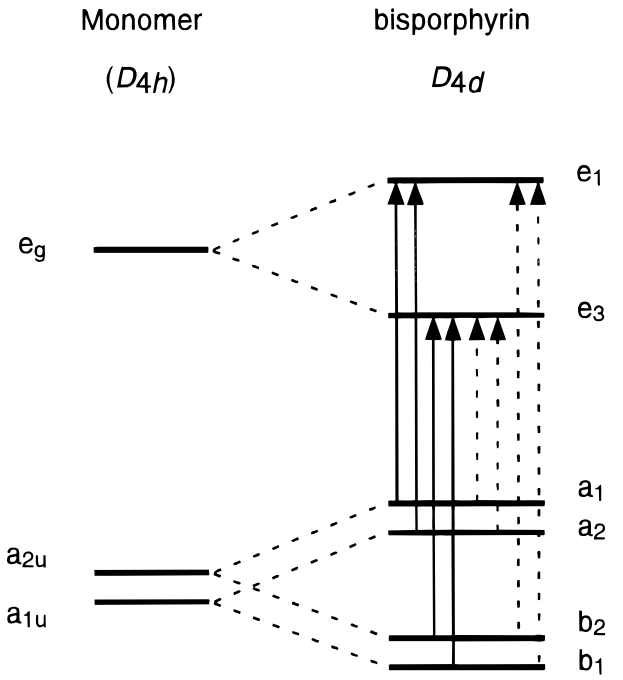

Figure 1. Schematic molecular orbital diagram of the supermolecule molecular orbitals (right side) formed from linear combinations of the 4-orbital MOs (left side) of the constituent monoporphyrin complexes. The solid arrows denote the dipole-allowed (E_1) one-electron transitions and the dashed arrows are used for the dipole-forbidden (E_3) one-electron transitions.

the eight orbitals of the sandwich (see Figure 1) results in four E_1 dipole-allowed and four E_3 dipole-forbidden excited state configurations in the pertinent D_{4d} symmetry. In the limit of degeneracy of the dipole-allowed configurations, (a_1e_1), (a_2e_1), (b_1e_3), and (b_2e_3), diagonalization of the CI matrix gives the singlet eigenfunctions B^+, Q^+, CR_1^+, and CR_2^+. The eigenfunctions B^+ and Q^+ are the allowed exciton states formed by in-phase combinations of the locally excited (intraligand) B and Q states of monomer subunits; CR_1^+ and CR_2^+ are the allowed charge resonance (CR) states formed by in-phase combinations of the interligand charge-transfer configurations. These wave functions provide a good description of the optical properties of the porphyrin double deckers. Indeed, the pure exciton B^+ and Q^+ states account for the nearly unperturbed (with respect to the monoporphyrin) B and Q bands, whereas the CR^+ states account for the new Q″ band. The CR character of the Q″ band is consistent with the observed sensitivity of the energy and intensity of this band to the ionic radius of the metal ion, that is, to the macrocycle separation. The four dipole-forbidden E_3 states have essentially mixed exciton and CR character. The lowest in energy, which is largely derived from the (a_1e_3) and (a_2e_3) configurations, is associated with the low-energy Q′ absorption. It has been recently shown that optical properties of porphyrin triple deckers can be understood by extending the supermolecule MO/CI picture developed for the double deckers.[31]

As for the heteroleptic sandwiches, their optical spectra are usually interpreted by analogy with the corresponding homosandwiches. The only theoretical investigation available is a semiempirical CI study in LO basis of Lu(Nc)(Pc) (Nc = 2,3-naphthalocyanine; Pc = phthalocyanine).[28]

An accurate description of the excited states of heteroleptic systems is not only of great general interest but also may shed light on the nonlinear optical properties of these electronically asymmetric strongly coupled systems.[20,21]

For the recently synthesized heteroleptic compound, Zr(OEP)(OEPz) (OEP = octaethylporphyrin, OEPz = octaethylporphyrazine), large first hyperpolarizabilities, β^{SHG}, were measured in an electric field induced second-harmonic generation (EFISH) experiment.[20] This is somewhat surprising as this molecule does not have the strong donor−acceptor structure of the push−pull porphyrinic systems, which are among the best performing NLO materials,[44] and it is only slightly asymmetric (in a homoleptic sandwich compound, the first hyperpolarizability vanishes on symmetry grounds). It is therefore important to understand the origin of this behavior theoretically.

In this paper, the excited states and the nonlinear optical properties (NLO) of this compound, which is the first heteroleptic sandwich whose second-order nonlinear optical properties (NLO) have been measured,[20] are studied using time-dependent density functional theory (TDDFT).

Contrary to the semiempirical approaches by which these systems have been studied before, TDDFT provides a first principles theory, which only recently has enabled the study of excitation energies, oscillator strengths, and (nonlinear) polarizabilities of systems of such size. TDDFT usually provides an accuracy for excitation energies which exceeds that of the CI singles method and is often comparable in accuracy to the most advanced other ab initio approaches.[43,45,46]

Very recently, molecular frequency-dependent hyperpolarizabilities have also become accessible in TDDFT.[47−50] The primary aim of this ongoing project was to provide a reliable first principles method (including the important effects of frequency dispersion and electron correlation) that is efficient enough to deal with molecules of the size considered here. Alternative correlated ab initio methods are prohibitively expensive for systems of this size. Semiempirical approaches are computationally cheap, on the other hand, but were unable to reproduce the experimental trends for other porphyrin systems.[51] An alternative method could be the time-dependent Hartree−Fock, although handling transition metal compounds is problematic for a method that does not include correlation effects.

Accurate theoretical calculations of the dynamic hyperpolarizability next to measurements are very important in view of the difficulties which occur on the experimental side. An example is given by our first application of TDDFT, in which our results on the dynamic hyperpolarizability of C_{60} confirmed the experimental data of Geng et al.,[52] who reported values that were orders of magnitude smaller than previous authors. Our conclusions are also confirmed by the most recent theoretical[53] and experimental[54] evidence.

For small molecules, the TDDFT calculations reproduce the experimental trends well[47] or very well. [55,56] The only known case in which the NLO TDDFT calculations are currently unsatisfactory[50] is, by now, well-understood[57] and is not believed to be relevant here, as it occurs for very long linear chains. In view of the following, it is important to note that with the approximations made in this work, one would expect, a priori, a (slight) overestimation for our theoretical hyperpolarizability results.

2. Method and Computational Details

The computational method we use is based on the time-dependent extension of density functional theory.[58−60] The solution of the TDDFT response equations proceeds in an iterative fashion, starting from the usual ground-state or zeroth-order Kohn−Sham (KS) equations. For these, one needs an approximation to the usual static exchange-correlation potential

$v_{xc}(\mathbf{r})$. After the ordinary KS equations have been solved, the first-order density change has to be calculated from an iterative solution to the first-order KS equations.[60] In these first-order equations, an approximation is needed to the first functional derivative of the time-dependent xc potential $v_{xc}(\mathbf{r}, t)$ with respect to the time-dependent density $\rho(\mathbf{r}',t')$.[47,48,59] For the analytic determination of the first hyperpolarizability, β, one additionally needs the second functional derivative g_{xc}. These so-called xc kernels, given by the equations

$$f_{xc}(\mathbf{r}, \mathbf{r}', t, t') = \frac{\delta v_{xc}(\mathbf{r}, t)}{\delta \rho(\mathbf{r}', t')} \quad (1)$$

$$g_{xc}(\mathbf{r}, \mathbf{r}', \mathbf{r}'', t, t', t'') = \frac{\delta^2 v_{xc}(\mathbf{r}, t)}{\delta \rho(\mathbf{r}', t') \delta \rho(\mathbf{r}'', t'')} \quad (2)$$

determine the exchange-correlation part of the screening of the externally applied electric field. Here, we use the so-called adiabatic local density approximation (ALDA) for the kernels. In this approximation (used almost without exception in the previously mentioned applications of TDDFT), the time dependence (or frequency dependence if one talks about the Fourier transformed kernel) is neglected, and one simply uses the differentiated static LDA expression derived from the homogeneous electron gas. In our case, we use the Vosko−Wilk−Nusair parametrization.[61] There is strong evidence[55,62] that the approximations made for f_{xc} and g_{xc} are usually of minor importance compared to the approximation made for v_{xc}, for which we use the generalized gradient approximated potentials (GGA) by Becke (for exchange)[63] and Perdew (for correlation),[64] BP.

All calculations reported in this paper have been performed with the ADF-RESPONSE module,[60] which is an extension of the Amsterdam density functional (ADF) program system.[65−67]

For the calculations, we made use of the standard ADF IV basis set,[68] which is an uncontracted triple-ζ STO basis set with one 3d polarization function for the C and N atoms, one 2p polarization function for H, and a triple-ζ *n*d, $(n + 1)$s basis with one $(n + 1)$p function for Zr. The cores (C, O: 1s; Zr: 1s−3d) were kept frozen.

For hyperpolarizabilities and (high-lying) excitation energy studies on small molecules, such basis sets need to be extended with diffuse functions, to describe the outer molecular region. However, for the systems under study, the main effects are related to ordinary bound orbitals, which are well described with the used basis sets. The addition of diffuse functions is therefore not expected to change our results by any significant amount. Thus, we expect that the errors related to basis set incompleteness are small compared to the errors induced by other approximations.

All calculations have been performed for the C_{4v} optimized geometry of the model system Zr(P)(Pz) (P = porphyrin, Pz = porphyrazine). The orientation of the molecule is shown in Figure 2.

3. Ground-State Molecular and Electronic Structure

The tetrapyrrole sandwich complexes share two relevant structural features: (i) the tetrapyrrole rings adopt a staggered orientation with a staggering angle ranging from ∼37° to ∼45° that makes the coordination environment of each metal cation a slightly distorted square antiprism; (ii) both tetrapyrroles are domed and severely distorted, with the average dihedral angles of the pyrrole rings ranging from ∼7° to ∼11°. According to our quantitative energy analysis of the intradimer interactions in large- and small-ring metallotetrapyrrole-based dimers,[69,70] and in metallodithiolene-type dimers,[71] both the staggering and the doming of the adjacent units are dictated by the necessity to minimize the steric hindrance between the two macrocycles, which are held more closely by the metal than their van der Waals distance and can be traced to Pauli repulsion between occupied orbitals.

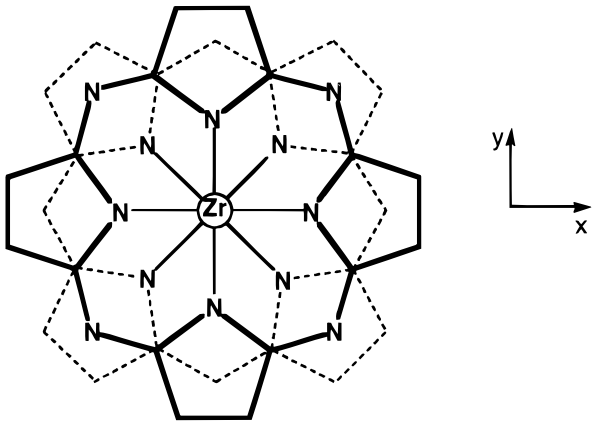

Figure 2. Configuration and orientation of Zr(P)(Pz) sandwich.

The above typical structural features are also present in the sandwich complex here investigated, Zr(OEP)(OEPz). According to the X-ray data reported by Collman et al.,[20] this complex shows a staggering angle of 42.4° and doming that is one of the most pronounced in porphyrin sandwiches. This is consistent with zirconium(IV) being one of the smallest metal ions known to form porphyrin sandwiches. Some of the most relevant experimental geometrical parameters of this complex and of the corresponding homo sandwiches, $Zr(OEP)_2$ and $Zr(OEPz)_2$, are listed in Table 1 together with the theoretical values calculated for the model Zr(P)(Pz) complex. Because the OEP subunit could not be distinguished from the OEPz subunit experimentally, the values reported in Table 1 are averages over the distances for the two porphyrins and do not help to clarify how the structural differences of the two macrocycles affect the geometrical parameters. Thus, in view of the well-documented accuracy of DFT calculations in predicting geometrical parameters of tetrapyrrole systems,[43,72] our theoretical data may provide more reliable information on this topic.

As inferred from the data in Table 1, the theoretical hole sizes of 4.095 Å for the porphyrin and of 3.898 Å for the azaporphyrin ring in the mixed model sandwich fit with the experimental values of 4.040 and 3.859 Å reported for the corresponding homo sandwiches $Zr(OEP)_2$ and $Zr(OEPz)_2$, respectively. This suggests that the contraction of the coordination cavity on going from porphyrin to azaporphyrin, already observed in monoporphyrins and in homo sandwiches, still holds in the mixed sandwich.

According to our calculations, the distances from the zirconium to the four pyrrolic nitrogens of P and Pz ($Zr-N_{av}$) are very similar, that is, 2.371 and 2.395 Å. Although the distance from the zirconium to the four pyrrolic nitrogens of the porphyrin ring matches the experimental value of 2.383 Å in $Zr(OEP)_2$ very well, the distance from the zirconium to the four pyrrolic nitrogens of the azaporphyrin ring is too large compared to the value of 2.308 Å in $Zr(OEPz)_2$. A similar discrepancy exists between the theoretical and experimental $Zr-N_{center}$ values. The calculated distance between the zirconium and the center of gravity of the four coordinated pyrrolic nitrogens of the Pz ring is indeed ∼0.08 Å larger than in $Zr(OEPz)_2$.

TABLE 1: Selected Average Bond Lengths (Å) and Metrical Parameters in Crystalline Zr(OEP)(OEPz), $Zr(OEP)_2$, and $Zr(OEPz)_2$ Compared with the Corresponding Theoretical, Optimized Values of the Model Zr(P)(Pz) Complex

param[a]	Zr(OEP)(OEPz)[b]	Zr(P)(Pz)[d]	$Zr(OEP)_2$[c]	$Zr(OEPz)_2$[b]
$Zr-N_{av}$[e]	2.342 (3, 5, 9, 8)	2.371, 2.395	2.383 (3, 5, 15, 8)	2.308 (3, 5, 10, 8)
N−N (hole size)[f]	3.946 (5, 10, 20, 4)	4.095, 3.898	4.040 (−, 10, 19, 4)	3.859 (4, 9, 18, 4)
$Zr-N_{center}$[g]	1.260, 1.262	1.243, 1.350	1.271, 1.260	1.270, 1.269

[a] For the experimental data, the bond lengths involving the metal atom and the porphyrin core have been averaged according to the idealized symmetry of the $Zr(Por)_2$ complex. The first number in parentheses following an average value of bond length is the root-mean-square estimated standard deviation of an individual datum. The second and third numbers, when given, are the average and maximum deviations from the averaged value, respectively. The fourth number represents the number of individual measurements which are included in the average value. [b] X-ray data at -60 ± 2 °C from ref 20. [c] X-ray data from ref 10. [d] The theoretical values of this work. The two entries for the listed geometrical parameters refer to the P and Pz rings, respectively. [e] The experimental $Zr-N_{av}$ values represent the average distance from the zirconium to the eight coordinated pyrrolic nitrogens. The theoretical $Zr-N_{av}$ values indicate the distance from the zirconium to the four pyrrolic nitrogens of P and Pz rings, respectively. [f] The hole size represents the distance between opposing coordinated nitrogens of a given macrocycle. [g] $Zr-N_{center}$ represents the distance from zirconium to the center-of-gravity for the four coordinated pyrrole nitrogens of the porphyrinic and porphyrazinic rings. The two entries for the experimental $Zr-N_{center}$ values account for the presence of two distinct porphyrin ligands for each of the sandwich complexes.

TABLE 2: One-electron Energies and Percentage Composition (Based on Mulliken Population Analysis per MO) of the Lowest Unoccupied and Highest Occupied Zr(P)(Pz) Orbitals in Terms of Zr, Pz, and P Fragments

	ϵ (eV)	Zr	P	Pz
		Unoccupied Orbitals		
$23a_1$	−1.90	79.0 ($4d_{z^2}$)	11.0 ($10a_1$)	10.0 ($10a_1$)
$15b_2$	−1.97			100.0 ($7b_2$)
31e	−2.76		87.0 (15e)	13.0 (15e)
30e	−3.41		13.0 (15e)	87.0 (15e)
		Occupied Orbitals		
$10a_2$	−4.63		59.0 ($5a_2$)	41.0 ($5a_2$)
$22a_1$	−4.95	4.0 ($4d_{z^2}$)	90.0 ($10a_1$)	5.0
$9a_2$	−5.47		41.0 ($5a_2$)	59.0 ($5a_2$)
$21a_1$	−5.79		43.0 ($9a_1$)	57.0 ($10a_1$)
$14b_2$	−5.82		91.0 ($7b_1$, $8b_1$)	9.0
29e	−5.88		75.0 (13e, 14e)	25.0 (14e)
$14b_1$	−5.93			100.0 ($8b_1$, $7b_1$)
$13b_2$	−5.97		10.0 ($7b_1$)	90.0 ($6b_2$)
28e	−6.19		15.0 (14e)	85.0 (13e, 14e)
27e	−6.35		13.0	87.0 (13e, 14e, 12e)
$20a_1$	−6.36		23.0 ($9a_1$)	77.0 ($9a_1$, $10a_1$)
26e	−6.76		84.0 (12e)	16.0 (11e)
$19a_1$	−6.76	7.0 ($4d_{z^2}$)	38.0 ($9a_1$)	54.0 ($9a_1$, $10a_1$)
$18a_1$	−7.02		2.0	98.0 ($8a_1$)

[a] The nature of contributions of more than 10% is reported in parentheses.

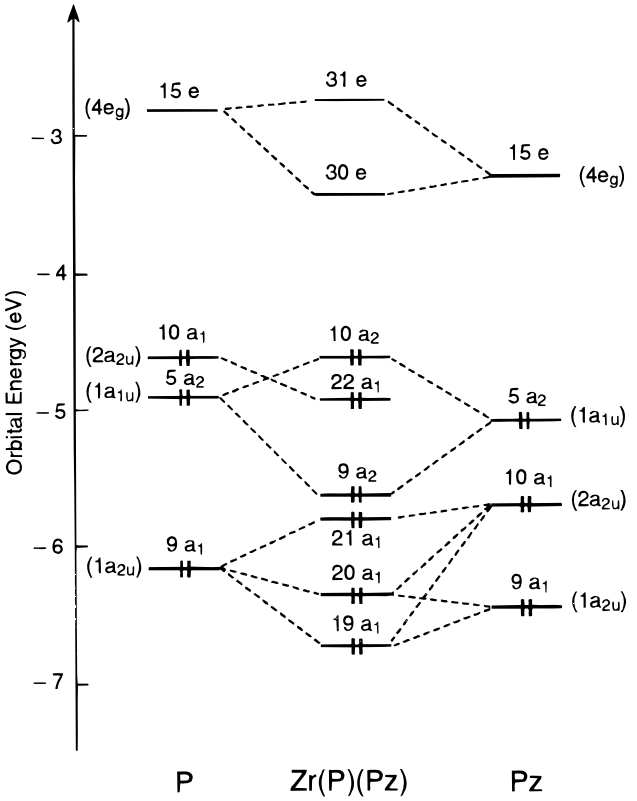

Figure 3. Interaction diagram of the highest occupied a_1 and a_2 and the lowest unoccupied e orbitals of the C_{4v} P and Pz subunits in Zr(P)(Pz). The parent D_{4h} names of the P and Pz fragment orbitals are also reported in parentheses. The P and Pz levels have been rigidly shifted to higher energies by 0.65 and 0.29 eV, respectively, to bring them into correspondence with the pure P and Pz MOs of the complex.

However, the experimental $Zr-N_{av}$ and $Zr-N_{center}$ geometrical parameters of $Zr(OEP)_2$ and $Zr(OEPz)_2$ are very well reproduced by our calculations on the model homo sandwiches $Zr(P)_2$ and $Zr(Pz)_2$, for which we predict $Zr-N_{av}$ values of 2.402 and 2.327 Å and $Zr-N_{center}$ values of 1.270 and 1.284 Å, respectively.[73] Thus, the above discrepancies are indicative of structural peculiarities of the mixed sandwich rather than failure of the calculations.

Before dealing with the UV−vis spectrum of Zr(P)(Pz), we will discuss the ground-state electronic structure of this molecule, in some detail, because the energy and composition of the MOs are a good tool to get a first insight into the nature of the excited states. To this end, we report in Table 2 the energy and composition of the highest occupied and lowest unoccupied MOs, in terms of Zr, P, and Pz fragment orbitals.

In discussing the orbital composition, it should be kept in mind that the order and position of the $1a_{1u}$ and $2a_{2u}$ orbitals change in going from P to Pz. The order depicted in Figure 1, with the $2a_{2u}$ above and close to the $1a_{1u}$, holds for P. The effect of introducing aza bridges stabilizes all levels, but preferentially stabilizes the $2a_{2u}$, which moves to considerably below the $1a_{1u}$ in Pz. This correlates with the $2a_{2u}$ having a high amplitude and the $1a_{1u}$ having nodes on the aza bridges (cf. discussion and orbital diagram in ref 70). According to the P/Pz orbital interaction diagram in Figure 3, the $1a_{1u}$ orbitals of P and Pz do exhibit some energy mismatch, but not nearly as strongly as the $2a_{2u}$ orbitals.

Among the four highest occupied molecular orbitals, the $10a_2$ (HOMO) and the $9a_2$ are the in-phase antibonding and out-of-phase bonding combinations of the $5a_2$ ($1a_{1u}$ in the D_{4h} ground-state symmetry of the bare macrocycles) orbitals of the porphyrin and azaporphyrin macrocycles. The quite large $10a_2/9a_2$ energy gap (0.84 eV) is indicative of strong $\pi-\pi$ interaction between the $5a_2$ π orbitals of the P and Pz subunits. This correlates with these orbitals having large amplitudes (more than 70%) on the C_α atoms that are eclipsed at the staggering angle of 45° and well within the van der Waals contact (3.15 Å in our optimized structure) in both rings. Because the $5a_2$ is in Pz, lower than in

P, the bonding combination of these orbitals ($9a_2$) has more weight on Pz and the antibonding combination ($10a_2$) has more weight on P.

The Pz and P $10a_1$ orbitals ($2a_{2u}$ in the D_{4h} ground-state symmetry of the bare macrocycles) are also suitable for interaction on the basis of their spatial characteristics. They indeed have large amplitudes on the pyrrolic nitrogens and on the bridge atoms (see plots of the $2a_{2u}$ and $1a_{1u}$ orbitals in ref 70), and although the 45° rotation angle staggers the nitrogen atoms on opposite rings, these atoms are still in close proximity (3.01 Å in our optimized structure). The pyrrolic nitrogens on one ring and the bridge atoms on the other ring are also quite close (3.25 Å in our optimized structure). However, the $2a_{2u}$-derived orbitals of the Pz and P macrocycles of the heteroleptic Zr(P)(Pz) sandwich do not interact. Unlike the corresponding homosandwiches, $Zr(OEP)_2$ and $Zr(OEPz)_2$, in which we find[73] that strong interactions between the monomers result in the bonding and antibonding $11b_2$ and $11a_1$ pair in the pertinent D_{4d} symmetry point group (see the scheme of Figure 1). The $2a_{2u}$-derived $10a_1$ orbital of the porphyrin ring is found almost purely (82%) in the $22a_1$, and the $2a_{2u}$-derived $10a_1$ of the azaporphyrin ring is found largely (57%) in the $21a_1$, where it mixes in *antibonding* fashion with the lower lying $9a_1$ orbital of the porphyrin ($1a_{2u}$ in the D_{4h} ground-state symmetry of the bare macrocycle), rather than with the $10a_1$. The bonding partner of the $21a_1$ is spread over the lower lying $19a_1$ and $20a_1$ MOs, which also contain the $1a_{2u}$-derived $9a_1$ Pz orbital. The strong localization of the $2a_{2u}$-derived $10a_1$ orbitals on either of the two macrocycles is due to energy mismatch.

According to the MO compositions reported in Table 2, the lower lying occupied orbitals, except for the $19a_1$ and $20a_1$, are strongly localized on either of the tetrapyrrolic rings, indicating that the P and Pz subunits have little interaction. As a matter of fact, the $14b_2$, the 26e, and the 29e MOs have a predominantly porphyrin character; the remaining MOs are mainly localized on the azaporphyrin ring. Concerning the character of the P based MOs, $14b_2$ is largely a pyrrolic nitrogen (N_p), C_β π orbital ($7b_1$), 26e is largely (84%) a π orbital delocalized on C_α, C_β, and bridging carbon (C_b) atoms, and 29e is a mixture of the porphyrin 13e and 14e N_p lone pairs.

As for the Pz-based orbitals, $14b_1$ is a mixture of Np lone pairs ($8b_1$) and the N_p, C_β ($7b_1$) π orbital. The $13b_2$ and $18a_1$ orbitals are the b_2 combination of bridging nitrogen (N_b) lone pairs and the a_1 combination of N_p lone pairs, respectively. Orbitals 27e and 28e are mixtures of the azaporphyrin ring 13e and 14e orbitals, the former being a π orbital localized on N_p and C_b atoms and the latter being the *e* combination of the N_p lone pairs.

Of the virtual orbitals listed in Table 2, 30e and 31e are the out-of-phase bonding and in-phase antibonding combinations of the P and Pz 15e orbitals ($4e_g$ in the D_{4h} ground-state symmetry of the bare macrocycles). Because of the lower energy of Pz levels compared to the P levels, 30e is localized on Pz and 31e on P. The next MO, the $15b_2$ is a pure Pz π orbital. The highest virtual orbital reported in Table 2, the $23a_1$, is a nearly pure metal orbital (78% Zr-$4d_{z2}$). The remaining metal orbitals (not shown in Table 2) lie at higher energy in the virtual spectrum because they are pushed up by strong interactions with the rings. The d_{xy} and $d_{x^2-y^2}$ orbitals interact with the pyrrolic nitrogen $2p_z$ orbitals of porphyrin and porphyrazine rings, respectively, and are found largely (more than 60%) in the $16b_1$ and $16b_2$ virtual MOs. The d_{xz} and d_{yz} pairs lie at even higher energy in the virtual spectrum, because of very strong σ-antibonding interactions with the P and Pz N_p lone pairs.

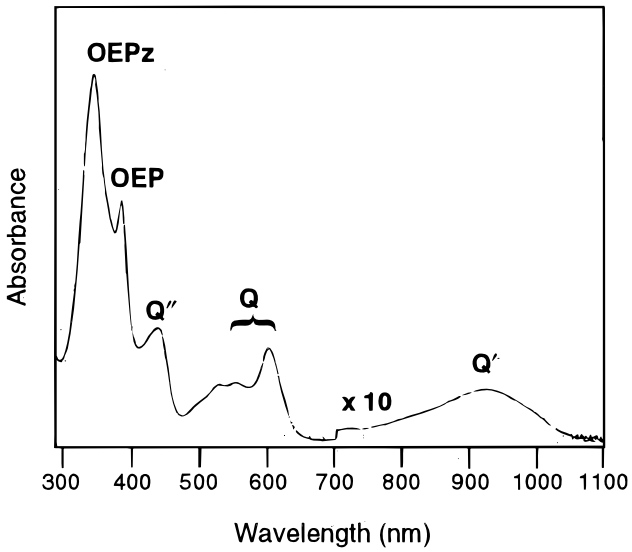

Figure 4. UV−vis spectrum of Zr(OEP)(OEPz) in dichloromethane from ref 20.

It should be noted that the interactions of occupied ring orbitals with empty metal orbitals are just the interactions that hold the two macrocycles together. The $\pi-\pi$ interactions between the P and Pz subunits all consist of two-orbital four-electron destabilizing interactions.

A relevant point which arises from our calculations is that on going from the bisporphyrin to the porphyrin/azaporphyrin mixed sandwich the energy and character of the MOs derived from bonding and antibonding interactions of the $1a_{1u}$, $2a_{2u}$, and $4e_g$ monomer orbitals change significantly. In bisporphyrins, they are indeed delocalized on both rings, whereas in the mixed sandwich, owing to the different electronic structure of the macrocycles, the $1a_{1u}$- and the $4e_g$-derived P and Pz orbitals make bonding and antibonding combinations which are strongly localized on either of the two rings, and the $2a_{2u}$-derived P and Pz orbitals do not mix at all. This reflects on the nature and energy of the excited states involving these orbitals, as discussed below.

4. Excited States and Optical Spectrum

The solution UV−vis spectrum of Zr(OEP)(OEPz) (see Figure 4) shows the typical features of heteroleptic sandwich complexes.[15] In the normal Q-band region of monoporphyrins, there are two absorptions, at 2.07 and 2.25 eV, and a shoulder at 2.38 eV. A weak broad band, the Q′ band, with a maximum at 1.34 eV and a Q″ band at 2.88 eV appear to the red and blue of the Q set, respectively. The UV region shows two intense bands, at 3.28 and 3.69 eV, the identities of which have been assigned by Collman et al.[20] on the basis of the Soret bands in the corresponding homosandwiches, that is, the absorption at 3.28 eV to the OEP subunit and the absorption at 3.69 eV to the OEPz subunit.

The excitation energies and oscillator strengths calculated for the lowest optically allowed ^1E and $^1A_1$ states are presented in Table 3 and compared with the experimental energy values determined from the solution spectrum of Zr(OEP)(OEPz). Table 3 also includes the composition of the BP/ALDA solution vectors in terms of the major one-electron MO transitions.

Our theoretical approach precludes a description of the excited states in terms of intraligand local transitions, referred to as excitonic (EX), and interligand cross-excitations, referred to as charge transfer (CT). Such a description, used extensively in

TABLE 3: Calculated Excitation Energies (eV) and Oscillator Strengths (*f*) for the Lowest Optically Allowed E and A_1 Excited States of Zr(P)(Pz) Compared to the Experimental Data

		Theory		Experiment[a]	
state	composition	energy	*f*	energy	assignment
1^1E	93% ($10a_2 \rightarrow 30e$)	1.39	0.0056	1.34	Q′
2^1E	96% ($22a_1 \rightarrow 30e$)	1.59	0.0003		
3^1E	73% ($10a_2 \rightarrow 31e$); 16% ($9a_2 \rightarrow 30e$)	2.02	0.0110	2.07	Q
4^1E	44% ($9a_2 \rightarrow 30e$); 23% ($21a_1 \rightarrow 30e$); 23% ($22a_1 \rightarrow 31e$)	2.33	0.0318	2.25	
5^1E	95% ($14b_2 \rightarrow 30e$)	2.43	0.0026	2.38 (sh)	
6^1E	49% ($21a_1 \rightarrow 30e$); 25% ($22a_1 \rightarrow 31e$); 13% ($9a_2 \rightarrow 31e$)	2.52	0.0032		
2^1A_1	98% ($29e \rightarrow 30e$)	2.53	0.0061		
7^1E	95% ($13b_2 \rightarrow 30e$)	2.60	0.0003		
8^1E	86% ($14b_1 \rightarrow 30e$)	2.63	0.000 01		
9^1E	24% ($20a_1 \rightarrow 30e$); 20% ($9a_2 \rightarrow 31e$); 18% ($9a_2 \rightarrow 30e$); 11% ($22a_1 \rightarrow 31e$)	2.73	0.1638	2.88	Q″
3^1A_1	94% ($28e \rightarrow 30e$)	2.91	0.0002		
4^1A_1	96% ($27e \rightarrow 30e$)	3.03	0.000 03		
10^1E	77% ($21a_1 \rightarrow 31e$); 12% ($9a_2 \rightarrow 31e$)	3.04	0.0377		
11^1E	41% ($14b_2 \rightarrow 31e$); 16% ($9a_2 \rightarrow 31e$); 12% ($20a_1 \rightarrow 30e$); 10% ($13b_2 \rightarrow 31e$)	3.15	0.0208		
12^1E	32% ($14b_2 \rightarrow 31e$); 22% ($9a_2 \rightarrow 31e$) 17% ($13b_2 \rightarrow 31e$); 11% ($20a_1 \rightarrow 30e$)	3.17	0.0492	3.28	B_1
13^1E	96% ($14b_1 \rightarrow 31e$)	3.19	0.0001		
5^1A_1	90% ($22a_1 \rightarrow 23a_1$)	3.24	0.0208		
14^1E	73%($13b_2 \rightarrow 31e$) ; 25%($14b_2 \rightarrow 31e$)	3.25	0.0044		
6^1A_1	90% ($29e \rightarrow 31e$)	3.26	0.0300		
7^1A_1	92% ($26e \rightarrow 30e$)	3.39	0.0027		
15^1E	96% ($19a_1 \rightarrow 30e$)	3.42	0.0244		
5^1A_1	84% ($28e \rightarrow 31e$)	3.49	0.0012		
16^1E	25% ($20a_1 \rightarrow 30e$); 14% ($18a_1 \rightarrow 30e$); 11%($21a_1 \rightarrow 31e$)	3.57	0.9820	3.69	B_2
17^1E	72% ($18a_1 \rightarrow 30e$); 19% ($20a_1 \rightarrow 31e$)	3.68	0.1084		

[a] From ref 20.

previous works on double- and triple-decker sandwiches,[2,27−31] would require the one-electron transitions contributing to the excited-state wavevectors to be expressed in terms of the localized fragment orbitals, rather than in terms of supermolecule orbitals, as they actually are expressed.

Nevertheless, our fragment formalism, according to which the supermolecule MOs are built up from Pz, P, and Zr fragment orbitals with the percentages given in Table 2, will still give indications as to the intra and/or interligand nature of the one-electron transitions that contribute to a given excited state.

According to the computed excitation energies and oscillator strengths, the very weak Q′ band is assigned to the 1^1E state. This assignment accounts very well for the breadth of the Q′ absorption. Because the 1^1E state is largely derived from the promotion of one electron from the antibonding $10a_2$ to the bonding 30e, there should be a displacement along the inter-macrocycle distance coordinate of the potential surface of the 1^1E state, relative to the ground state, leading to a shift of the Franck−Condon intensity from the origin to higher vibronic components and a broad absorption contour. This may also explain the low intensity of the Q′ absorption, which, unlike in the corresponding homosandwiches, is dipole-allowed in the mixed sandwich, due to the lowering of the $D_{4d} \rightarrow C_{4v}$ symmetry. The shift of the potential energy surface relative to that of the ground state may lead to the dispersal of intensity over higher vibronic components.

In the energy regime of the Q′ band, we find another excited state, the 2^1E, which, given its very small oscillator strength, only contributes to the broadening of this band.

Because the 1^1E and 2^1E states are dominated by transitions which are from a delocalized orbital (the $10a_2$ HOMO with 59% P character) and from a nearly pure porphyrin orbital ($22a_1$) to a largely Pz orbital, respectively, the Q′ band has a predominant P → Pz interligand character, with a minor Pz → Pz and P → P intraligand contribution. A mixed exciton and CR character has also been suggested[2] for the Q′ band of the bisporphyrins. However, the mixed character of the Q′ band has a very different origin in each case. While the mixed character of the Q′ band in the porphyrin/azaporphyrin sandwich is a direct consequence of the different electronic structures of the P and Pz subunits, it was traced[2] to the nondegeneracy of the appropriate E_3 basis configurations in the bisporphyrins, that is, the (a_1e_3) and (a_2e_3) and the (b_1e_1) and (b_2e_1) pairs of configurations (see Figure 1).

In the energy regime of the Q-band system (2.0−2.6 eV) we find six ^1E and one $^1A_1$ excited states. The 3^1E and 4^1E excited states, calculated at 2.02 and 2.33 eV, nicely account for the two absorptions of the Q envelope at 2.07 and 2.25 eV, whereas the 5^1E, the 6^1E, and the 2^1A_1 excited states, calculated at 2.43, 2.52, and 2.53 eV, respectively, account for the higher energy shoulder at 2.38 eV. The very weak and nearly degenerate 7^1E and 8^1E states, calculated at 2.60 and 2.63 eV, contribute to the broadening of the Q-band system at the border with the Q″ band.

However, the relative magnitudes of the oscillator strengths of the 3^1E and 4^1E excited states are calculated in reverse order with respect to the experiment. The absorption at 2.07 eV in the Q envelope is indeed about two times more intense than the one at 2.25 eV.

The discrepancy between the calculated and observed intensity ratios of the 3^1E and 4^1E states might be caused by an incorrect determination by TDDFT of the coefficients of the one-electron transitions, which give the major contribution to the oscillator strengths.

It should be mentioned, however, that the composition and the oscillator strengths of these two states show a strong geometric dependence. Using a slightly different geometry, obtained by optimization of the molecule with a smaller basis set for the ligand atoms, we find a 75% contribution of the $10a_2 \rightarrow 31e$ and a 15% contribution of the $9a_2 \rightarrow 30e$ for the 3^1E, and for the 4^1E we find a 46% contribution of the $21a_1 \rightarrow 30e$, a 33% contribution of $9a_2 \rightarrow 30e$, and a 14% contribution of $22a_1 \rightarrow 31e$. The oscillator strengths are 0.0172 and 0.0166 for 3^1E and 4^1E, respectively, which are more in line with the observed intensities.

Therefore, if one considers that our calculations are performed on a model system and the comparison is made with a solution and not with a gas-phase spectrum, the discrepancy between the calculated and observed intensity ratios of the 3^1E and 4^1E states is perfectly understandable.

According to the composition of the excited-state wavevectors, the 3^1E, the 4^1E, and the 6^1E have a multitransition character and involve transitions from the four highest occupied to the two lowest unoccupied molecular orbitals.

We find a 73% contribution for the $10a_2 \rightarrow 31e$ (P, Pz→P) one-electron transition and a 16% for the $9a_2 \rightarrow 30e$ (Pz, P → Pz) in the solution vector of the 3^1E. The $21a_1 \rightarrow 30e$ (Pz, P → Pz) and $22a_1 \rightarrow 31e$ (P → P) transitions are strongly mixed in the 4^1E and 6^1E states, in which we also find contributions from the $9a_2 \rightarrow 30e$ and $9a_2 \rightarrow 31e$ (Pz, P → P), respectively. From the wavevector composition of the excited states lying in the Q region, it is clear that the Q-band system has a predominant intraligand character, although there is considerable mixture with interligand excitation. It is worth noting that there are several excited states in the energy regime of the Q-band associated with n → π^* transitions that are from N_p or N_b lone pairs on either of the two rings to the 30e π^*. This is the case of the 5, 7, 8^1E, and 2^1A_1 excited states.

We should mention that for the assignment of the Q envelope, an alternative hypothesis is possible. The possibility is to consider the features at 2.25 and 2.38 eV as a vibronic progression of the prominent peak of the Q envelope to which both the 3^1E and 4^1E states should belong. The remaining, much weaker, excited states would then be responsible for the broadening of the higher energy tail of the Q-band system.

On the basis of the computed excitation energy and oscillator strength, the assignment of the Q″ band at 2.88 eV to the 9^1E state calculated at 2.73 eV is unambiguous. This state has a pronounced multitransition character. Indeed, we find large and comparable weights for the $20a_1 \rightarrow 30e$ (Pz → Pz), $9a_2 \rightarrow 31e$ (Pz, P → P), and $9a_2 \rightarrow 30e$ (Pz, P → Pz) excitations and smaller but significant weights for the $22a_1 \rightarrow 31e$ (P → P) and the $21a_1 \rightarrow 30e$ (Pz, P → Pz). According to our calculations, the Q″ band has considerable excitonic character.

In the energy regime of the two B bands centered at 3.28 and 3.69 eV, we find two sets of closely spaced excited states, spanning the 2.91−3.26 eV and 3.39−3.68 eV energy ranges. The summed oscillator strengths of 0.1630 and 1.1187 computed for the B_1 and B_2 bands nicely agree with the experimental relative intensities.

However, the individual oscillator strengths indicate that it is the 16^1E excited-state calculated at 3.57 eV which gives most of the intensity to the B band centered at 3.69 eV. The intensity of the lower energy B band is dispersed over a number of excited states, namely the 10^1E, 11^1E, and 12^1E and the 5^1A_1 and 6^1A_1.

As far as the character of the B_1 and B_2 bands is concerned, our calculations show that the B_2 has a dominant Pz → Pz intraligand character.

Indeed, we note that the excited states with the largest oscillator strengths, the 16^1E and the 17^1E, are dominated by the $20a_1 \rightarrow 30e$ and $18a_1 \rightarrow 30e$ one-electron transitions that are strongly localized on the Pz ring.

The character of the lower-lying B_1 band is less defined in our calculations, although the excited states with the largest oscillator strengths have a prevalent P → P intraligand character.

It should be noted that beyond the $\pi \rightarrow \pi^*$ transitions involving the four highest occupied and two lowest unoccupied MOs of the molecule, we find a number of transitions in the B-band region, a few of which contribute with large weights to the most intense excited states, which are from lower lying occupied MOs, such as the porphyrin $14b_2$ N_p lone pair, $13b_2$ N_b lone pair, and azaporphyrin $18a_1$ N_p lone pair. We also find the 5^1A_1, a ligand-to-metal charge transfer (LMCT) state in the B_1 band region, that is dominated by the $22a_1 \rightarrow 23a_1$ one-electron transition.

5. Hyperpolarizability Calculations

A measurement of the first hyperpolarizability β (-2ω; ω, ω) related to second-harmonic generation (SHG), using the EFISH technique, gave a result of $\beta = \beta_{vec} = (-83 \pm 43) \times 10^{-30}$ esu, where, for a molecule with its dipole moment along the *z*-axis, β_{vec} is given by

$$\beta_{vec} = \beta_z = \frac{1}{3} \sum_{\xi=x,y,z} (\beta_{z\xi\xi} + \beta_{\xi z\xi} + \beta_{\xi\xi z}) \qquad (3)$$

Assuming the validity of a simple two-state model, this was extrapolated to zero frequency, giving an estimated static value of β_{vec} (0; 0, 0) = $(-62 \pm 32) \times 10^{-30}$ esu. Such large hyperpolarizabilities are rarely observed, with the exception of the so-called "push−pull" molecules, which contain strong donor and acceptor groups. A further interesting outcome of the measurement is the negative value of the observed hyperpolarizability, implying a second-order decrease in the absolute value of the dipole moment upon laser irradiation. Molecules displaying large hyperpolarizabilities usually have positive hyperpolarizabilities. For these reasons, a detailed theoretical investigation is called for, because such calculations can aid us in understanding the origin of the sign and magnitude of the hyperpolarizability of this molecule, thereby rendering it possibe to reconcile the findings of the mentioned experiment with common intuition on the relationship between molecular structure and the magnitude of the NLO response.

TABLE 4: Theoretical Hyperpolarizabilities at Different Frequencies for Zr(P)(Pz) Compared with the Experimental Results for Zr(OEP)(OEPz)

frequency		$\beta^{SHG}(10^{-30}$esu$)^{a,b}$		$\beta^{EOPE}(10^{-30}$ esu$)^{c,b}$
au	eV	expt	BP/ALDA	BP/ALDA
0.000	0.000	$(-62 \pm 32)^d$	0.450	0.450
0.005	0.136		0.475	0.458
0.010	0.408		0.560	0.483
0.020	0.544		1.433	0.606
0.022	0.599		2.249	0.650
0.023 892 6	0.650	-83 ± 43^e	4.928	0.701
0.025	0.681		16.469	0.735
0.025 5	0.694		−251.62	0.752
0.026	0.708		−14.421	0.771
0.027	0.735		−4.880	0.810
0.028	0.762		−2.741	0.855
0.030	0.817		−2.021	0.963

[a] First hyperpolarizability related to Second Harmonic Generation effect. [b] All values reported in esu units, according to convention B* in ref 62; Conversion factor between au and esu units is given by 1 au = $8.639\,418 \times 10^{-33}$ esu. [c] First hyperpolarizability related to Electrooptic Pockels effect. [d] Extrapolation to zero frequency using a two state model, ref 20. [e] Value extracted from EFISH experiment at λ = 1907 nm in solution, ref 20.

In Table 4, our hyperpolarizability results are displayed at different photon energies (or wavelengths). Concentrating first on the static hyperpolarizability, we find a *relatively small, positive* value for β_{vec}, although the extrapolation from experiment gave rise to a *large, negative* value. The origin of this discrepancy can be understood from the results at higher frequencies. There, the theoretical hyperpolarizability results increase strongly as the pole of β (-2ω; ω, ω) at $\omega = 0.69$ eV is approached. Directly after this pole, which is quite close to the laser frequency of $\omega = 0.65$ eV ($\lambda = 1907$ nm) that was used, β_{vec} attains large and negative values, in perfect agreement with the experimental findings. No artificial damping parameters have been included in the calculations, which means that β_{vec} can attain arbitrarily large positive and negative values near a pole. Therefore, a quantitative comparison to the experimental values in this frequency range is not meaningful. However, the general *shape* of the curve (large and positive before the pole,

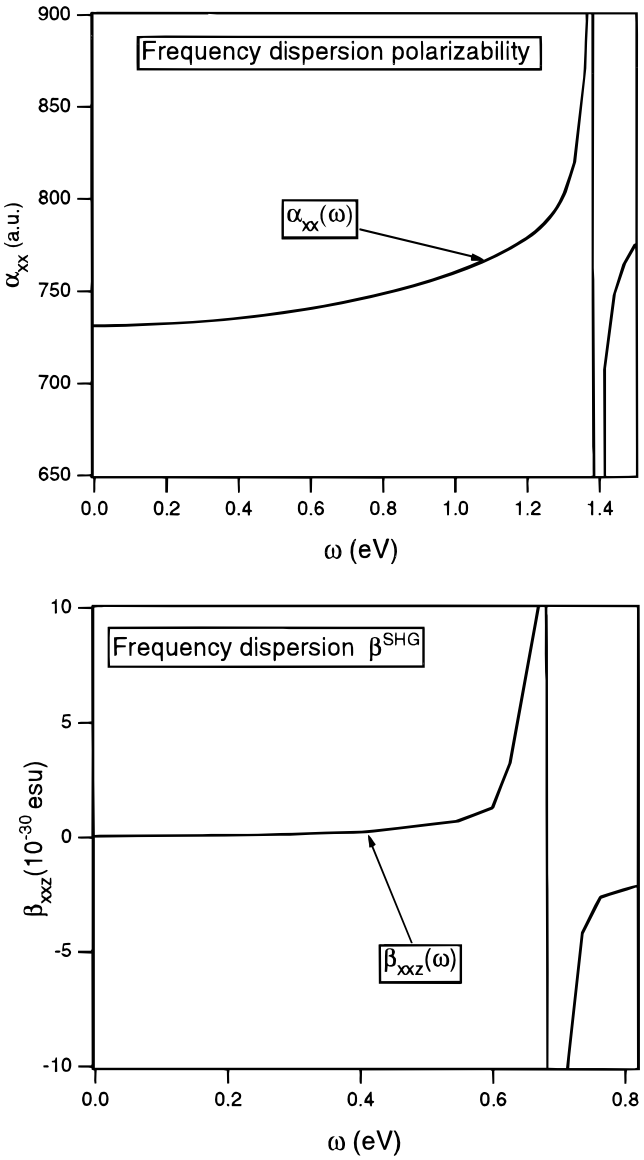

Figure 5. Frequency-dependent polarizability component $\alpha_{xx}(\omega)$ (Top) and hyperpolarizability component $\beta_{xxz}(\omega)$ (Bottom) of Zr(P)(Pz) sandwich.

large and negative after the pole) should be trustworthy. If we analyze β_{vec} in terms of the individual tensor components β_{ijk}, we find that the strong frequency dependence near $\omega = 0.69$ eV originates from the components β_{xxz} and β_{yyz}, which are identical with respect to symmetry. The component β_{zzz}, on the other hand, remains close to its zero frequency value. In Figure 5, β_{xxz} is displayed as a function of the frequency, together with the related linear polarizability component α_{xx} (which is identical to α_{yy}, the dipole moment being in the *z* direction.). As noted above, β_{xxz} has a pole near $\omega = 0.69$ eV. This pole is related to the pole at $\omega = 1.39$ eV in α_{xx}. From sum-over-states expressions for the hyperpolarizability tensor (see, for example, refs 48 and 59), one immediately notes that a pole in α shows up in the β^{SHG} expression as a pole at half of this frequency. The pole in α is due to the Q′ excitation energy, for which we found a theoretical value of 1.39 eV, while the experimental estimate was 1.34 eV (cf. Table 3). In other words, the laser frequency of $\omega = 0.65$ eV (1907 nm) used in the EFISH experiment was quite close to half the experimental excitation energy of 1.34 eV (2×0.65 eV $= 1.30$ eV). This was acknowledged in ref 20, but its significance may have been underestimated.

In comparing theoretical and experimental hyperpolarizabilities, one has to practice extreme care, as several conventions are in use. In Table 4, we present our results in convention B* (cf. ref 62), which is the most common convention for experiments using the dc-SHG technique (it is assumed that this convention was also adopted in ref 20, although the chosen convention was not explicitly mentioned in that work). The numbers in an alternative convention, based upon a Taylor expansion of the dipole moment (this is convention AB or T in ref 62), are the ones most used by ab initio theoreticians working on small molecules and can be obtained by multiplying all β values in Table 4 by a factor of 6. The difference in conventions is, thus, simply a constant factor, the sign of the hyperpolarizability or the steepness of its frequency dependence does not depend on the chosen convention.

With regard to the two-state model, used in ref 20 to extrapolate the results to zero frequency, we can say that our results show that this procedure is not reliable because of the closeness of the pole. If a few-state model is applied in this case, one would certainly have to take into account the close-lying Q′ pole, in addition to states that are much further away in energy, such as the Q″ excitation used in ref 20.

It should be emphasized that in the present work we have calculated the electronic gas-phase hyperpolarizability. It is well-known that vibrational[74] and solvent effects are important additional factors. Vibrational contributions can sometimes be of a magnitude similar to, or even larger than, their electronic counterparts. The influence of the solvent can be even more drastic as it sometimes changes the sign of the hyperpolarizability.[75] The effects of the solvent are known to be especially large when, as in this case, polar solvents are used.

These effects may easily double or triple the electronic values presented here. However, our most important conclusions concern the frequency dependence and pole structures, which are unaffected by those additional effects. The changes induced by the solvent are often related to changes induced in the absorption spectrum (often the excitation energies in the solvent are lower and the hyperpolarizabilities are larger). In our case, the theoretical Q′ excitation energy is found to be quite close to the experimental value in the solvent. Therefore, we expect the influence of the solvent to be relatively small in this case. It is more difficult to make an estimate for the magnitude of the vibrational contribution to β.

We conclude that both the sign and the magnitude of the hyperpolarizability of Zr(OEP)(OEPz) may be related to resonance effects due to the Q′ band.

6. Conclusions

In this paper, we have investigated the linear and nonlinear optical properties of the recently synthesized Zr(OEP)(OEPz) mixed sandwich, using a TDDFT approach. The excited states and oscillator strengths calculated for the model complex, Zr(P)(Pz), reproduce the salient features of the UV−vis spectrum of the complex, the so-called Q′, Q, Q″, B_1, and B_2 bands very well. This yields further evidence of the usefulness of this method for excitation energies, which is relatively inexpensive, but often comparable in accuracy to the most advanced other ab initio approaches, as proven in the case of the free base porphin[43] and transition metal complexes.[45,46] The nature of the excited states has been described in terms of intraligand (excitonic) and interligand (charge transfer) transitions and interpreted in the light of the electronic structure of the complex.

From our analysis of the excited states, it becomes evident that, due to the different electronic structures of the P and Pz subunits, the origin and the character of the Q′, Q, Q″, and B bands of the mixed P/Pz complex are different compared to that of the bisporphyrin analogue.

The usefulness of the efficient implementation of TDDFT for response properties[76] has been demonstrated in the present theoretical investigation of $\beta(-2\omega; \omega, \omega)$ at various values of ω. It has enabled us to identify the measured large negative β^{SHG} at $\omega = 0.65$ eV as a special result caused by the proximity of a pole in β (calculated at 0.69 eV).

The off-resonance values of β^{SHG} are not large. At low frequencies, including the static value (0.45×10^{-30} esu), they are positive and uninterestingly small.

References and Notes

(1) For a review, see: Deisenhofer, J.; Michel, H. *Science* **1989**, *245*, 1463.

(2) Bilsel, O.; Rodriguez, J.; Milam, S. N.; Gorlin, P. A.; Girolami, G. S.; Suslick, K. S.; Holten, D. *J. Am. Chem. Soc.* **1992**, *114*, 6528.

(3) Buchler, J. W.; De Cian, A.; Fischer, J.; Kihn-Botulinski, M.; Paulus, H.; Weiss, R. *J. Am. Chem. Soc.* **1986**, *108*, 3652.

(4) Buchler, J. W.; Elsässer, K.; Kihn-Botulinski, M.; Scharbert, B. *Angew. Chem., Int. Ed. Engl.* **1986**, *25*, 286.

(5) Buchler, J. W.; Hüttermann, J.; Löffler, J. *Bull. Chem. Soc. Jpn.* **1988**, *61*, 71.

(6) Buchler, J. W.; De Cian, A.; Fischer, J.; Kihn-Botulinski, M.; Weiss, R. *Inorg. Chem.* **1988**, *27*, 339.

(7) Buchler, J. W.; Scharbert, B. *J. Am. Chem. Soc.* **1988**, *110*, 4272.

(8) Buchler, J. W.; De Cian, A.; Fischer, J.; Hammerschmitt, P.; Löffler, J.; Scharbert, B.; Weiss, R. *Chem. Ber.* **1989**, *122*, 2219.

(9) Buchler, J. W.; De Cian, A.; Fisher, J.; Hammerschmitt, P.; Weiss, R. *Chem. Ber.* **1991**, *124*, 1051.

(10) Buchler, J. W.; De Cian, A.; Elschner, S.; Fischer, J.; Hammerschmitt, P.; Weiss, R. *Chem. Ber.* **1992**, *125*, 107.

(11) Buchler, J. W.; Kihn-Botulinski, M.; Löffler, J.; Scharbert, B. *New. J. Chem.* **1992**, *16*, 545.

(12) De Cian, A.; Moussavi, M.; Fischer, J.; Weiss, R. *Inorg. Chem.* **1985**, *24*, 3162.

(13) Girolami, G. S.; Milam, S. N.; Suslick, K. S. *Inorg. Chem.* **1987**, *26*, 343.

(14) Girolami, G. S.; Milam, S. M.; Suslick, K. S. *J. Am. Chem. Soc.* **1988**, *110*, 2011.

(15) Kadish, K. M.; Moninot, G.; Hu, Y.; Dubois, D.; Ibnlfassi, A.; Barbe, J.-M.; Guilard, R. *J. Am. Chem. Soc.* **1993**, *115*, 8153.

(16) Kim, K.; Lee, W. S.; Kim, H.-J.; Cho, S.-H.; Girolami, G. S.; Gorlin, P. A.; Suslick, K. S. *Inorg. Chem.* **1991**, *30*, 2652.

(17) Kim, H.-J.; Whang, D.; Kim, J.; Kim, K. *Inorg. Chem.* **1992**, *31*, 3882.

(18) Buchler, J. W.; Löffler, J. *Z. Naturforsch* **1990**, *45b*, 531.

(19) Chabach, D.; Tahiri, M.; De Cian, A.; Fischer, J.; Weiss, R.; El Malouli Bibout, M. *J. Am. Chem. Soc.* **1995**, *117*, 8548.

(20) Collman, J. P.; Kendall, J. L.; Chen, J. L.; Eberspacher, T. A.; Moylan, C. R. *Inorg. Chem.* **1997**, *36*, 5603.

(21) Girolami, G. S.; Gorlin, P. A.; Suslick, K. S. *Inorg. Chem.* **1994**, *33*, 626.

(22) Guilard, R.; Barbe, J.-M.; Ibnlfassi, A.; Zrineh, A.; Adamian, V. A.; Kadish, K. M. *Inorg. Chem.* **1995**, *34*, 1472.

(23) Lachkar, M.; De Cian, A.; Fischer, J.; Weiss, R. *New. J. Chem.* **1988**, *12*, 729.

(24) Ng, D. K. P.; Jiang, J. *Chem. Soc. Rev.* **1997**, *26*, 433.

(25) Spiroulias, G. A.; Coutsolelos, A. G. *Inorg. Chem.* **1996**, *35*, 1382.

(26) Spyroulias, G. A.; Coutsolelos, A. G.; Raptopoulou, C. P.; Terzis, A. *Inorg. Chem.* **1995**, *34*, 2476.

(27) Ishikawa, N.; Ohno, O.; Kaizu, Y.; Kobayashi, H. *J. Phys. Chem.* **1992**, *96*, 8832.

(28) Ishikawa, N.; Ohno, O.; Kaizu, Y. *J. Phys. Chem.* **1993**, *97*, 1004.

(29) Ishikawa, N.; Kaizu, Y. *J. Phys. Chem.* **1996**, *100*, 8722.

(30) Bilsel, O.; Buchler, J. W.; Hammerschmitt, P.; Rodriguez, J.; Holten, D. *Chem. Phys. Lett.* **1991**, *182*, 415.

(31) Wittmer, L. L.; Holten, D. *J. Phys. Chem.* **1996**, *100*, 860.

(32) Donohoe, R. J.; Duchowski, J. K.; Bocian, D. F. *J. Am. Chem. Soc.* **1988**, *110*, 6119.

(33) Duchowski, J. K.; Bocian, D. F. *J. Am. Chem. Soc.* **1990**, *112*, 3312.

(34) Perng, J.-H.; Duchowski, J. K.; Bocian, D. F. *J. Phys. Chem.* **1990**, *94*, 6684.

(35) Chandra, A. C.; Lim, E. C. *J. Phys. Chem.* **1968**, *48*, 2589.

(36) Koutecky, J.; Paldus, J. *Collect. Czech. Chem. Commun.* **1962**, *27*, 599.

(37) Scherer, P. O. J.; Fischer, S. F. *Chem. Phys.* **1989**, *131*, 115.

(38) Thompson, M. A.; Zerner, M.; Fajer, J. *J. Phys. Chem.* **1991**, *95*, 5693.

(39) Gouterman, M. *J. Chem. Phys.* **1959**, *30*, 1139.

(40) Gouterman, M. In *The Porphyrins*; Dolphin, D., Ed.; Academic Press: New York, 1978; Vol. III, Part A, pp 1−165.

(41) Serrano-Andrés, L.; Merchán, M.; Rubio, M.; Roos, B. O. *Chem. Phys. Lett.* **1998**, *295*, 195.

(42) Rubio, M.; Roos, B. O.; Serrano-Andrés, L.; Merchán, M. *J. Chem. Phys.* **1999**, *15*, 7202.

(43) van Gisbergen, S. J. A.; Rosa, A.; Ricciardi, G.; Baerends, E. J. *J. Chem. Phys.* **1999**, *111*, 2499.

(44) Le Cours, S. M.; Guan, H.-W.; Di Magno, S. G.; Wangand, C. H.; Therien, M. J. *J. Am. Chem. Soc.* **1996**, *118*, 1497.

(45) van Gisbergen, S. J. A.; Groeneveld, J. A.; Rosa, A.; Snijders, J. G.; Baerends, E. J. *J. Phys. Chem. A* **1999**, *103*, 6835.

(46) Rosa, A.; Baerends, E. J.; van Gisbergen, S. J. A.; van Lenthe, E.; Groeneveld, J. A.; Snijders, J. G. *J. Am. Chem. Soc.* **1999**, *121*, 10356.

(47) van Gisbergen, S. J. A.; Snijders, J. G.; Baerends, E. J. *J. Chem. Phys.* **1998**, *109*, 10644.

(48) van Gisbergen, S. J. A.; Snijders, J. G.; Baerends, E. J. *Phys. Rev. Lett.* **1997**, *78*, 3097−3100.

(49) van Gisbergen, S. J. A.; Snijders, J. G.; Baerends, E. J. *J. Chem. Phys.* **1998**, *109*, 10657.

(50) Champagne, B.; Perpète, E. A.; van Gisbergen, S. J. A.; Baerends, E. J.; Snijders, J. G.; Soubra-Ghaoui, C.; Robins, K.; Kirtman, B. *J. Chem. Phys.* **1998**, *109*, 10498.

(51) Pryadarshy, S.; Therien, M. J.; Beratan, D. N. *J. Am. Chem. Soc.* **1996**, *118*, 1504.

(52) Geng, L.; Wright, J. C. *Chem. Phys. Lett.* **1996**, *249*, 105.

(53) Norman, P.; Luo, Y.; Jonsson, D.; Ågreen, H. *J. Chem. Phys.* **1997**, *106*, 8788.

(54) Li, J.; Wang, S.; Yang, H.; Gong, Q.; An, X.; Chen, H.; Qiang, D. *Chem. Phys. Lett.* **1998**, *288*, 175.

(55) Schipper, P. R. T.; Gritsenko, O. V.; van Gisbergen, S. J. A.; Baerends, E. J., submitted for publication.

(56) Cohen, A. J.; Handy, N. C.; Tozer, D. J. *Chem. Phys. Lett.* **1999**, *303*, 391.

(57) van Gisbergen, S. J. A.; Schipper, P. R. T.; Gritsenko, O. V.; Baerends, E. J.; Snijders, J. G.; Champagne, B.; Kirtman, B., submitted for publication.

(58) Casida, M. Time Dependent Density Functional Response Theory for Molecules In *Recent Advances in Density Functional Methods*; Chong, D. P., Ed.; World Scientific: Singapore, 1995; Vol. 1; p 155.

(59) Gross, E. U. K.; Dobson, J. F.; Petersilka, M. In *Density Functional Theory*; Nalewajski, R. F., Ed.; Springer Series Topics in Current Chemistry; Springer: Heidelberg, 1996.

(60) van Gisbergen, S. J. A.; Snijders, J. G.; Baerends, E. J. *Comput. Phys.* **1999**, *118*, 119.

(61) Vosko, S. H.; Wilk, L.; Nusair, M. *Can. J. Phys.* **1980**, *58*, 1200.

(62) Willetts, A.; E., R. J.; Burland, D. M.; Shelton, D. P. *J. Chem. Phys.* **1992**, *97*, 7590.

(63) Becke, A. *Phys. Rev. A* **1988**, *38*, 3098.

(64) Perdew, J. P. *Phys. Rev. B* **1986**, *33*, 8822 (Erratum: PRB 8834 1986 7406).

(65) Baerends, E. J.; Ellis, D. E.; Ros, P. *Chem. Phys.* **1973**, *2*, 41.

(66) te Velde, G.; Baerends, E. J. *J. Comput. Phys.* **1992**, *99*, 84.

(67) Fonseca Guerra, C.; Visser, O.; Snijders, J. G.; te Velde, G.; Baerends, E. J. Parallelisation of the Amsterdam Density Functional Program. In *Methods and Techniques for Computational Chemistry*; Clementi, E., Corongiu, G., Eds.; STEF: Cagliari, 1995; pp 305−395.

(68) ADF STO basis set database available on line at http://tc.chem.vu.nl/SCM/Doc/atomicdatabase.

(69) Rosa, A.; Baerends, E. J. *Inorg. Chem.* **1992**, *31*, 4717.

(70) Rosa, A.; Baerends, E. J. *Inorg. Chem.* **1993**, *32*, 5637.

(71) Rosa, A.; Ricciardi, G.; Baerends, E. J. *Inorg. Chem.* **1998**, *37*, 1368.

(72) Ghosh, A. *Acc. Chem. Res.* **1998**, *31*, 189.

(73) Rosa, A.; Ricciardi, G.; Baerends, E. J., manuscript in preparation.

(74) Bishop, D. M. *Adv. Chem. Phys.* **1998**, *140*, 1.

(75) Mikkelsen, K. V.; Luo, Y.; Ågreen, H.; Jørgensen, P. *J. Chem. Phys.* **1995**, *102*, 9362.

(76) van Gisbergen, S. J. A. Molecular Response Property Calculations Using Time-Dependent Density Functional Theory. Ph.D. Thesis, Vrije Universiteit, 1998.